View Aliasing Artifacts Reduction Method Based on 4D Cone-Beam CT Reconstruction with Joint Projection Data

Shaohua Zhi, Xuanqin Mou

***Abstract*—Although the quality of the phase-resolved reconstruction images could be improved by the four-dimensional cone-beam computed tomography (4D-CBCT) by reducing the motion blurring artifacts, it may still be degraded by severe view-aliasing artifacts because of highly under-sampled projections at each phase. Inspired by the strong correlation between different phase-resolved reconstructed images, we present a simple and effective approach to estimate a set of full-sampled projections for every individual respiratory phase and then to incorporate them into the 4D-CBCT iterative reconstruction scheme. In the implementation of the 4D-CBCT iterative reconstruction scheme, a coupled distance-driven forward and backward projection operator via GPU is introduced. The proposed method has been tested in a digital XCAT phantom and a clinical patient case. Quantitative evaluations indicate that a 15.7% and 9.9% decrease in the root-mean-square error (RMSE) are achieved by our method when comparing with the conventional 4D-CBCT reconstruction method and the classic McKinnon/Bates algorithm (MKB), respectively. At the same time, our method is also valid by calculating the contrast-to-noise ratio (CNR) of a region of interest (ROI). The result shows that the CNR of our method is 1.34, which is better than that of the MKB algorithm.**

***Index Terms*—Cone-Beam CT, 4D-CBCT Reconstruction, MKB algorithm, Joint projection data**

I. Introduction

CBCT has been clinically used to verify the patient position, localize the target of treatment and offer possibilities to update the treatment protocol in the image-guided radiation therapy (IGRT) [1]. However, due to the rotational speed limitations of kV imaging systems on linear accelerator gentries, the conventional CBCT acquisition gives rise to motion blurring problems of moving organs. 4D-CBCT reconstruction technique [2] has been recently developed to overcome the shortcomings. In 4D-CBCT, the acquired full-sampled projections are sorted into different groups corresponding to various breathing phases and to reconstruct the phase-resolved images independently. Nevertheless, under-sampling streaking artifacts are present in the reconstructed images, and the image contrast resolution is also significantly compromised. Moreover, the projection views for a certain phase in 4D-CBCT are usually clustered into several groups with a larger angular spacing between projections [3]. Consequently, the low efficiency of the bunched sampling pattern leads to an increasing artifacts level when comparing with the uniform sampling pattern in most conventional few-view problems in CT Fig. 1.

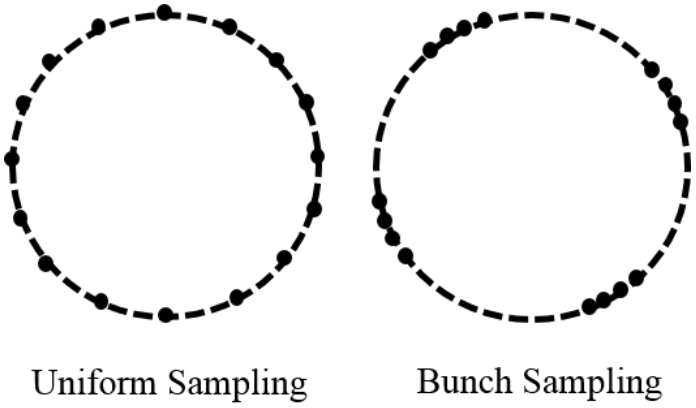

Fig. 1. The uniformed sampling pattern and the bunched sampling pattern.

Many efforts have been devoted to solve the data under-sampling problem in 4D-CBCT [4]–[7]. One strategy is to directly extract the motion affected volumetric images in projection domain by calculating the difference between the forward projection of a prior volumetric reconstruction and the measured projections(such as the MKB algorithm [8], [9] and its modified version [10]).

Although the MKB algorithm has the potential of suppressing view aliasing artifacts effectively and being implemented easily, it still suffers from low SNR and other artifacts [10] caused by the insufficient number of projection views and the inaccurate estimation of motion-compensated images. Base on observations that different phase-resolved images have strong interactions between each other, it can be assumed that the principal component of the motion variation among different phases can be well approximated by comparing the difference of interconnected phase-resolved reconstructions from one another.

Inspired by the assumption, we propose a simple but effective method for eliminating residual view aliasing artifacts by using the subtraction between different phase-resolved images in projection domain to generate a set of joint full-view projections for a single phase reconstruction. In addition, we also introduce a coupled distance-driven (DD) forward and backward projection operator [11], [12] via the GPU acceleration technique [13] in the implementation of the proposed

This work is partly supported by the National Natural Science Foundation of China (NSFC) (No. 61571359) and the National Key Research and Development Program of China (No. 2016YFA0202003).

The authors are with the Institute of Image processing and Pattern recognition, Xi'an Jiaotong University, Xi'an, Shaanxi 710049, China. (Email:zhishaohua.1203@stu.xjtu.edu.cn, xqmou@mail.xjtu.edu.cn)

DOI: 10.12059/Fully3D.2017-11-3202040

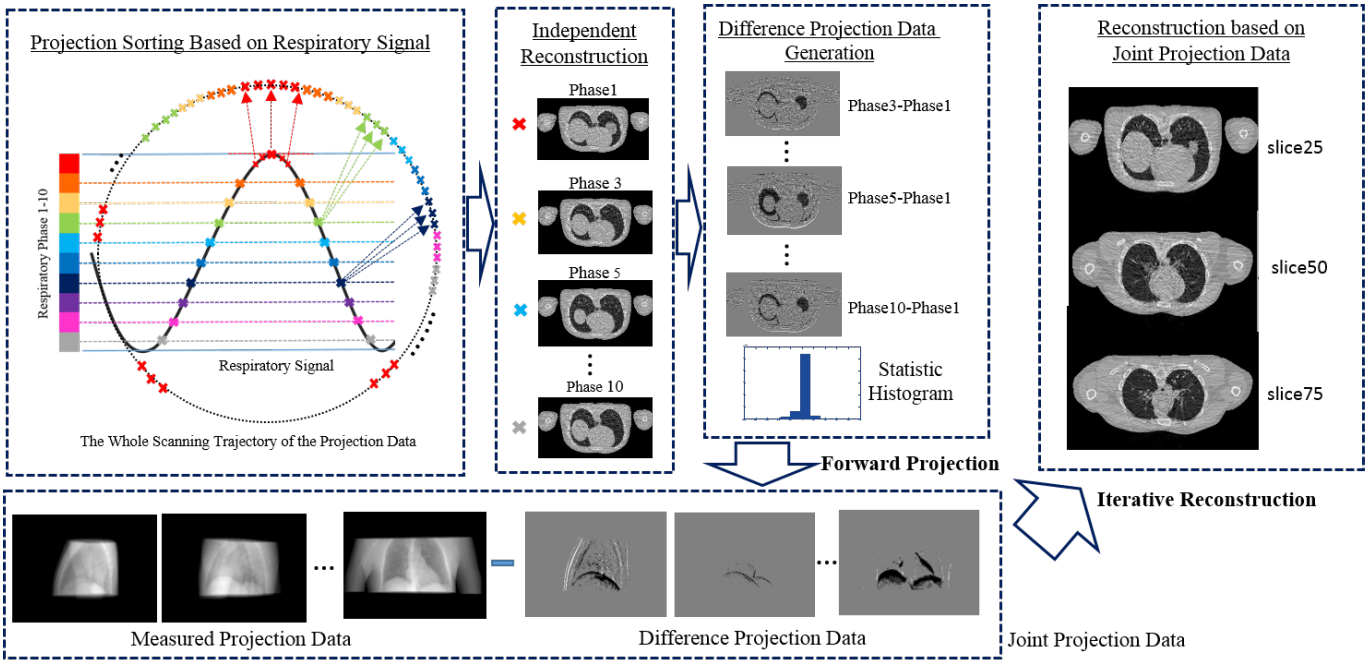

Fig. 2. The flowchart of the proposed method, which can be divided into independent phase-resolved reconstruction, difference projection data generation, and full-view joint projection completion followed by phase-resolved reconstruction.

4D-CBCT iterative reconstruction method.

II. Materials and Methods

A. The framework of the proposed method

The proposed method is organized in the following three steps: independent phase-resolved reconstruction, difference projection data generation, and full-view joint projection completion followed by phase-resolved reconstruction. The detailed flowchart for the proposed method is illustrated in Fig. 2.

1) Independent phase-resolved reconstruction: It is assumed that the breathing signal can be obtained from either external surrogate or respiratory signal extraction algorithms, accordingly the set of measured projection images can be classified into different n_t phase bins $\{j = 1, 2, \cdots, n_t\}$ (n_t is usually set to 10) with an expression of $P = \{P_j = A_j\mu_j + N_j, j \leq n_t\}$.

In this work, 4D-CBCT images $\{\mu_j | j = 1, 2, 3, \cdots, n_t\}$ at each phase j are reconstructed by an algebraic reconstruction technique (ART), which is posed by Eq. (1), where A_j represents the system matrix corresponding to the X-ray transform of the phase j.

$$\hat{\mu}_j = \arg\min_{\mu} \|A_j\mu_j - P_j\|_2^2 \tag{1}$$

2) Difference projection data generation: Based on the n_t phase-resolved volumetric images obtained in Section II-A1, $(n_t - 1)$ difference images are generated by subtracting the remaining $(n_t - 1)$ images from the 1st one.

Before the difference projection is achieved by forward-projection operator, we have applied statistic histograms for each difference images. It is shown that the peak value of every statistic histogram can reflect principle energy of the difference images especially for motion variation. Thus, an histogram based thresholding segmentation method is adopted to reduce the tiny difference caused by the anatomy background or the view-aliasing artifacts of the reconstruction.

3) Reconstruction using the full-view joint projection for each phase: Instead of insufficient projections sorted by gating technique for each phase, a set of joint full-view projections are generated by incorporating the residual projections into measured projections. Subsequently, the corresponding phase-resolved CBCT images can be reconstructed with no streaking artifacts .

B. Reconstruction algorithm based on coupled distance-driven projector pair

Projector and back-projector pair are used to refine an image estimation in iterative image reconstruction. The performance of an iterative reconstruction algorithm for X-ray tomography strongly relies on the match level and the type selection of tomographic operators [14]. Based on the fact that projector and back-projector pair are conducted many times in Section II-A1 and Section II-A3, a coupled distance-driven based tomographic projector is adopted to implement the 4D-CBCT iteration reconstruction scheme. Numerical experiments were carried out to explore the artifacts reduction performance and the degree of matching of projection operators by comparing the coupled DD operator with the uncoupled pixel-driven (PD) [12] and the ray-driven (RD) approaches [15], [16], respectively.

III. Numerical Experiments and Results Analysis

An XCAT phantom [17] and a real clinical case are both studied to evaluate the performance of our algorithm.

The XCAT phantom is at thorax region which can provide a realistic model of the human anatomy and can be used to simulate both cardiac and respiratory motion. The regular respiratory pattern is set to a period of 4 second while the heartbeat rhythm is set to a period of 0.8 second. Generally, the respiratory cycle is divided into 10 phases and the CBCT scanning time is 60 second with 600 projection images through 360° gantry rotation (full-fan scan mode). Hence, the number of projections for each respiratory phase is 60 views. The dimension of the phantom is 256×256×100 with an isotropic voxel size of 1 mm. The source-to-isocenter distance and the source-to-detector distance are 1000 mm and 1536 mm respectively. The X-ray detector size is 409.6×409.6 mm with the resolution 512×384 pixel^2.

For the real data, the patient is scanned by an Eleka XVI system (Elekta AB, Stockholm, Sweden) with a off-center positioned scanning protocols such that the iso-center focuses on the left lung. Total 1169 views of X-ray projections are acquired in 200 degree gantry rotation (short-scan mode) in 4 minute. The respiratory signal is obtained by Amsterdam Shroud method [18] because the scale of breathing condition can be precisely reflected by the motion of the thoracic diaphragm. The projections are grouped into ten phases according to the respiratory signal. The detector size is 409.6×409.6 mm^2 with the resolution of 512×512 pixel^2 in both dimensions. The source-to-isocenter distance and the source-to-detector distance are the same to that of the XCAT geometry. The reconstructed image volume is 256×256×256.

TABLE I
ROOTED-MEAN-SQUARE ERROR (RMSE)

RMSE	MKB	Proposed Method	DD	PD-RD
XCAT	6.3203	5.6946	6.7548	6.6293

TABLE II
CONTRAST-TO-NOISE RATIO (CNR)

CNR	MKB	Proposed Method	DD	PD-RD
NKI Data	0.9313	1.3379	0.7316	1.4016

1) Results: We first display the reconstructed 4D-CBCT volumetric images in Fig. 3 and Fig. 4 for the XCAT case and the patient case, respectively. As can be seen in Fig. 3, the 1st to the 3th column represent ground truth of the XCAT phantom at phase 1, the results of the proposed method and the results of MKB algorithm respectively. The 4th and the 5th columns are the conventional 4D reconstructions at phase 1 based on coupled DD projector and the uncoupled RD-PD projector, respectively. The three rows present the tomographic image at slice 25, 50, 70 of the reconstructed XCAT phantom. In Fig. 4, we present the results using four methods at transversal, coronal and sagittal views.

Due to inadequate X-ray projections in each phase, no matter whether the coupled DD projector or the uncoupled RD-PD projector is used or not, obvious streaking artifacts are observed in the conventional 4D reconstructions. Moreover, the images produced by the MKB algorithm have relatively more distinct anatomical structures when comparing with independent 4D reconstructions at different slices. However, the image quality of the motion-compensated reconstruction by the MKB method is deteriorate by streaking artifacts due to limited number of projections. In the 2nd column by the proposed method, those streaking artifacts appeared in the MKB algorithm are effectively suppressed with a arrow mark, while the anatomical features are well preserved.

In Fig. 4, the full-view reconstruction represents the image reconstructed by the whole measured projections with explicit static features while blurred dynamic features especially at the diaphragm location. It can be observed that the results of the proposed method have little streaking artifacts and more distinct reconstruction at the motion part compared with the other two methods.

2) Quantitative analysis: We use two quantitative metrics to assess the 4D-CBCT reconstructed image quality. The first assessment index is the RMSE for the XCAT simulated phantom. The results are shown in Table I. The second assessment index is the CNR, which is calculated as CNR $= 2|\mu - \mu_b|/(\sigma + \sigma_b)$, where μ and μ_b are the mean values in the ROI and in a nearby region considered as the background, respectively. It is for quantifying the tumor detection capability for a given ROI that is marked by a red circle in Fig. 4. σ and σ_b are the standard deviations of the pixel values inside the ROI and in the background. We have measured the CNRs in each phases and calculated the average CNR over all 10 phases. The results are shown in Table II.

Obviously both RMSE and CNR metrics can demonstrate that our proposed method is better than the conventional MKB algorithm.

IV. CONCLUSIONS

Inspired by the core idea of the MKB algorithm, we develop a simple but effective method with joint cone-beam projection images in the 4D-CBCT reconstruction algorithm. Our method is aiming to suppress the streaking artifacts caused by insufficient projections for each phase. Numerical simulation and clinical data proves its effectiveness in alleviating this kind of artifacts. Our method is better than the conventional MKB algorithm and 4D independent reconstruction method according to both qualitative analysis and quantitative evaluation. Moreover, a coupled DD projector is adopted into the proposed method to avoid the error caused by mismatches of forward and backward projector. As can been seen from the convergence curve in Fig. 5, the RMSE value of coupled DD projector is far lower than that of uncoupled PD-RD projector.It indicates that the coupled DD projector based has the ability of yielding superior reconstructions then the other tomographic projectors.

However, our method can be further improved in two aspects. On one hand, the spatial resolution of the bronchi with the feature of branches of trees is not improved so much, which may have an influence on the correct position of tumor near the areas. It is expected that by further exploring the full potential of the correlation between temporal phases, this drawback could be remedied.

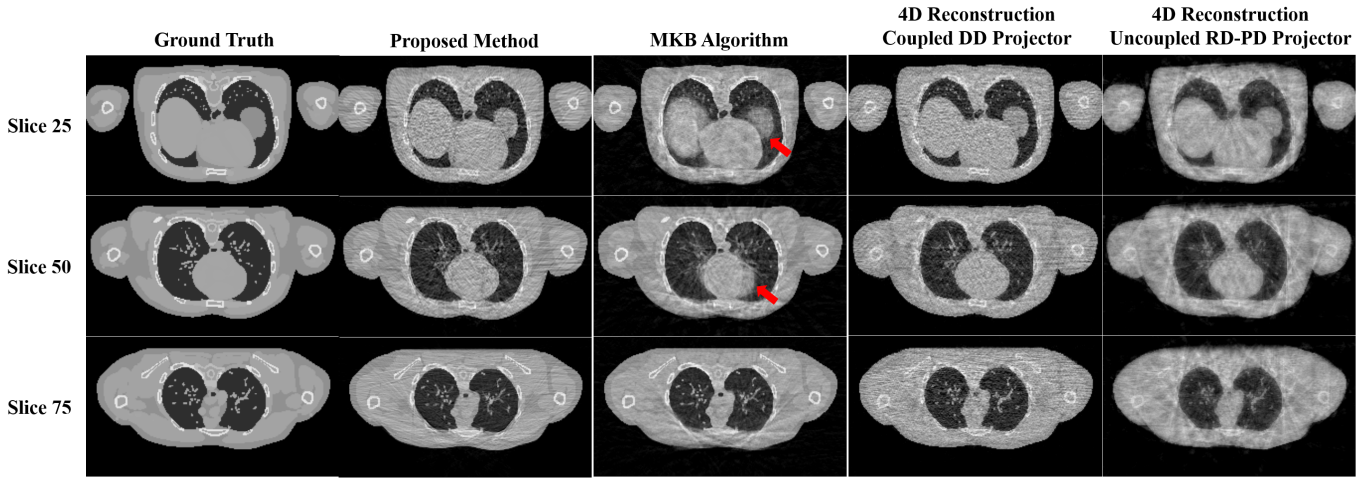

Fig. 3. Ground truth as well as reconstruction of the simulated XCAT phantom using different reconstruction techniques. The gray scale window is [0.005, 0.035].

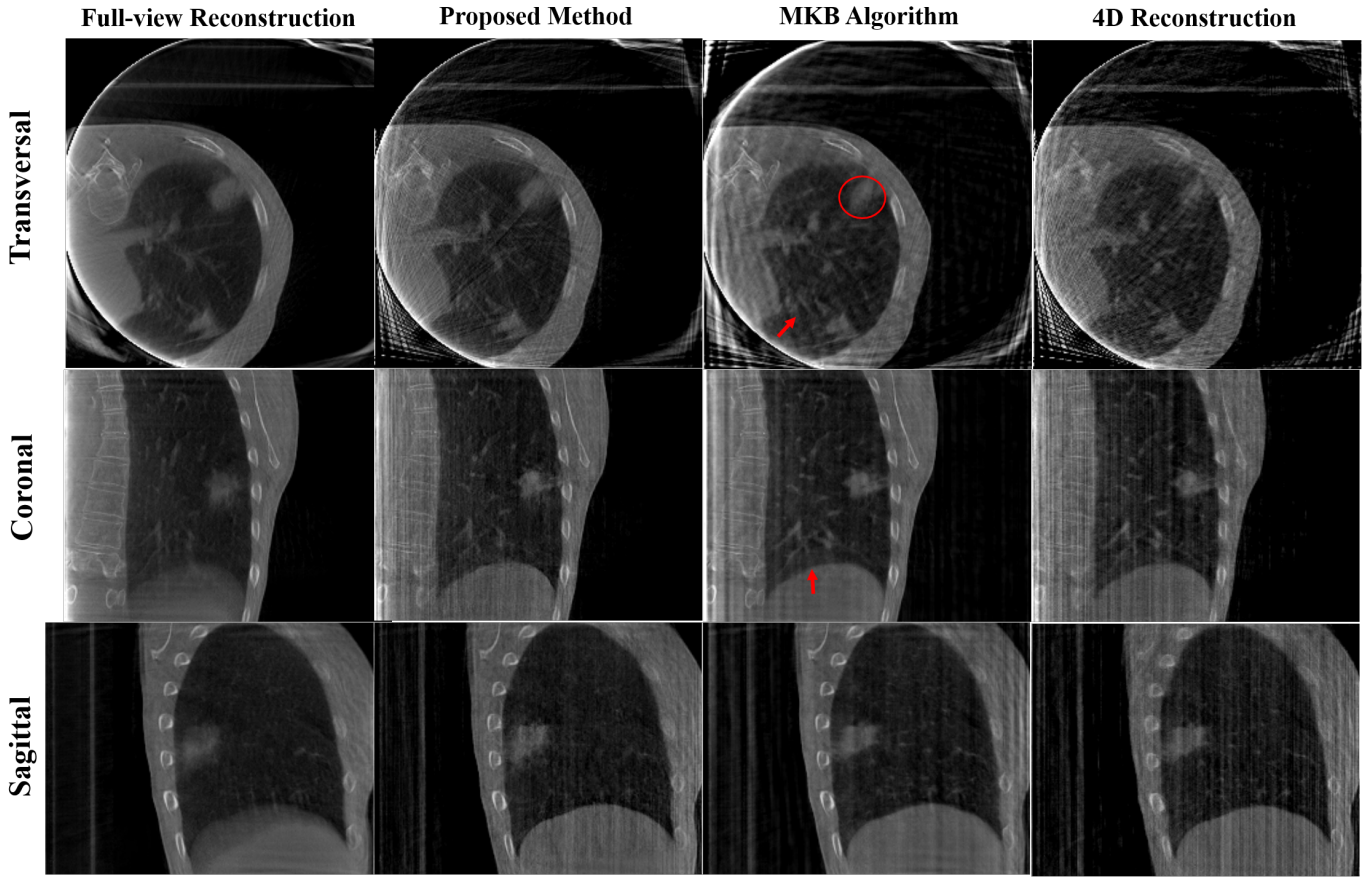

Fig. 4. 4D-CBCT images of NKI real patient data at first phase bin. A transversal (top row), a coronal (middle row), and a sagittal view (bottom row) are displayed. The prior volumetric reconstruction without phase binning (first column left), the reconstruction of the proposed method (the second colume left), the MKB algorithm based reconstruction (third column, middle) as well as the phase-resolved reconstruction by ART (fourth column left) are presented. The red circle indicates the ROI of the tumor-like structure used to evaluate the CNR while the red arrows present the improvements of our method. The gray scale window is [0.005, 0.035].

On other hand, the frequency of using forward and backward projection operators in our method is high, so we should draw support from the GPU acceleration, and thus its computational efficiency need to be discussed in our further research.

REFERENCES

[1] D. A. Jaffray, J. H. Siewerdsen, J. W. Wong, and A. A. Martinez, "Flat-panel cone-beam computed tomography for image-guided radiation therapy," *International Journal of Radiation Oncology*Biology*Physics*, vol. 53, no. 5, pp. 1337 – 1349, 2002.

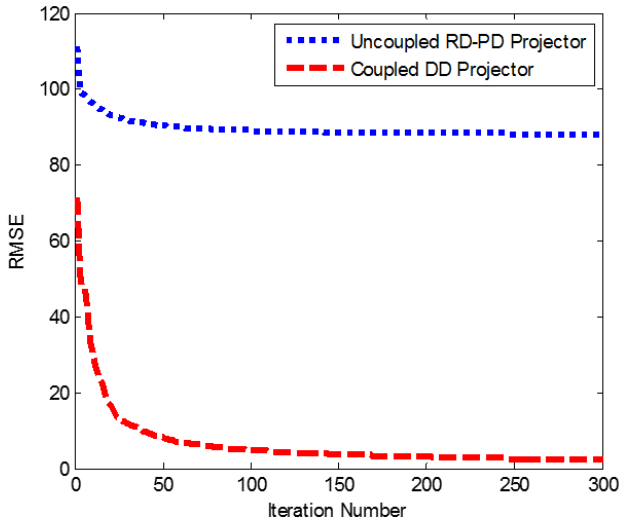

Fig. 5. The convergence curves of coupled DD projection operator based reconstruction (red dashed line) and uncoupled PD-RD projection operator based reconstruction(blue dashed line).

[2] J.-J. Sonke, L. Zijp, P. Remeijer, and M. van Herk, "Respiratory correlated cone beam ct," *Medical Physics*, vol. 32, no. 4, pp. 1176–1186, 2005.

[3] M. Brehm, P. Paysan, M. Oelhafen, P. Kunz, and M. Kachelrie, "Self-adapting cyclic registration for motion-compensated cone-beam ct in image-guided radiation therapy," *Medical Physics*, vol. 39, no. 12, pp. 7603–7618, 2012.

[4] J. Wang and X. Gu, "High-quality four-dimensional cone-beam ct by deforming prior images," *Physics in Medicine and Biology*, vol. 58, no. 2, p. 231, 2013.

[5] G.-H. Chen, J. Tang, and S. Leng, "Prior image constrained compressed sensing (piccs): A method to accurately reconstruct dynamic ct images from highly undersampled projection data sets," *Medical Physics*, vol. 35, no. 2, pp. 660–663, 2008.

[6] X. Jia, Z. Tian, Y. Lou, J.-J. Sonke, and S. B. Jiang, "Four-dimensional cone beam ct reconstruction and enhancement using a temporal nonlocal means method," *Medical Physics*, vol. 39, no. 9, pp. 5592–5602, 2012.

[7] H. Gao, J.-F. Cai, Z. Shen, and H. Zhao, "Robust principal component analysis-based four-dimensional computed tomography," *Physics in Medicine and Biology*, vol. 56, no. 11, p. 3181, 2011.

[8] K. L. Garden and R. A. Robb, "3-d reconstruction of the heart from few projections: A practical implementation of the mckinnon-bates algorithm," *IEEE Transactions on Medical Imaging*, vol. 5, no. 4, pp. 233–239, Dec 1986.

[9] S. Leng, J. Zambelli, R. Tolakanahalli, B. Nett, P. Munro, J. Star-Lack, B. Paliwal, and G.-H. Chen, "Streaking artifacts reduction in four-dimensional cone-beam computed tomography," *Medical Physics*, vol. 35, no. 10, pp. 4649–4659, 2008.

[10] Z. Zheng, M. Sun, J. Pavkovich, and J. Star-Lack, "Fast 4d cone-beam reconstruction using the mckinnon-bates algorithm with truncation correction and nonlinear filtering," in *Proc. SPIE 7961, Medical Imaging 2011: Physics of Medical Imaging*, N. J. Pelc, E. Samei, and R. M. Nishikawa, Eds., vol. 7961, March 2011, pp. 79 612U–79 612U–8.

[11] B. D. Man and S. Basu, "Distance-driven projection and backprojection in three dimensions," *Physics in Medicine and Biology*, vol. 49, no. 11, p. 2463, 2004.

[12] G. T. Herman, *Fundamentals of computerized tomography: image reconstruction from projections*. Springer Science & Business Media, 2009.

[13] L. Singaravelu, C. Pu, H. Hrtig, and C. Helmuth, "Reducing TCB Complexity for Security-sensitive Applications: Three Case Studies," in *Proceedings of the 1st ACM SIGOPS/EuroSys European Conference on Computer Systems 2006*, ser. EuroSys '06. New York, NY, USA: ACM, 2006, pp. 161–174.

[14] F. Arcadu, M. Stampanoni, and F. Marone, "On the crucial impact of the coupling projector-backprojector in iterative tomographic reconstruction," *arXiv preprint arXiv:1612.05515*, 2016.

[15] T. M. Peters, "Algorithms for fast back- and re-projection in computed tomography," *IEEE Transactions on Nuclear Science*, vol. 28, no. 4, pp. 3641–3647, Aug 1981.

[16] W. Zhuang, S. S. Gopal, and T. J. Hebert, "Numerical evaluation of methods for computing tomographic projections," *IEEE Transactions on Nuclear Science*, vol. 41, no. 4, pp. 1660–1665, Aug 1994.

[17] W. P. Segars, G. Sturgeon, S. Mendonca, J. Grimes, and B. M. W. Tsui, "4d xcat phantom for multimodality imaging research," *Medical Physics*, vol. 37, no. 9, pp. 4902–4915, 2010.

[18] J. Sonke, M. V. Herk, J. Belderbos, M. Rossi, A. Betgen, and J. Lebesque, "An off-line 4d cone beam ct based correction protocol for lung tumor motion," *International Journal of Radiation Oncology*Biology*Physics*, vol. 63, pp. S389–S390, 2005.